JACS
JOURNAL OF THE AMERICAN CHEMICAL SOCIETY

Article

pubs.acs.org/JACS

Single-Molecule Investigation of Initiation Dynamics of an Organometallic Catalyst

James D. Ng, Sunil P. Upadhyay, Angela N. Marquard, Katherine M. Lupo, Daniel A. Hinton, Nicolas A. Padilla, Desiree M. Bates, and Randall H. Goldsmith*

Department of Chemistry, The University of Wisconsin—Madison, 1101 University Avenue, Madison, Wisconsin 53706, United States

Supporting Information

ABSTRACT: The action of molecular catalysts comprises multiple microscopic kinetic steps whose nature is of central importance in determining catalyst activity and selectivity. Single-molecule microscopy enables the direct examination of these steps, including elucidation of molecule-to-molecule variability. Such molecular diversity is particularly important for the behavior of molecular catalysts supported at surfaces. We present the first combined investigation of the initiation dynamics of an operational palladium cross-coupling catalyst at the bulk and single-molecule levels, including under turnover conditions. Base-initiated kinetics reveal highly heterogeneous behavior indicative of diverse catalyst population. Unexpectedly, this distribution becomes more heterogeneous at increasing base concentration. We model this behavior with a two-step saturation mechanism and identify specific microscopic steps where chemical variability must exist in order to yield observed behavior. Critically, we reveal how structural diversity at a surface translates into heterogeneity in catalyst behavior, while demonstrating how single-molecule experiments can contribute to understanding of molecular catalysts.

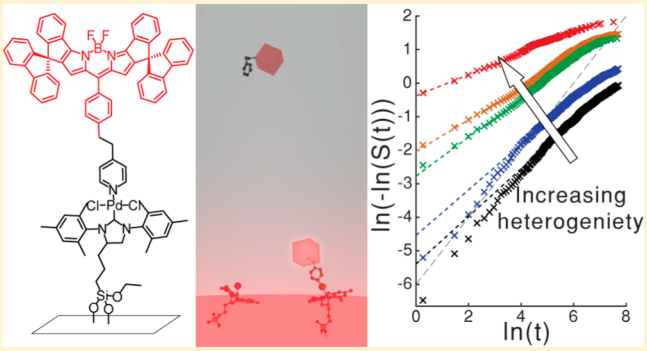

INTRODUCTION

Single-molecule (SM) fluorescence microscopy is a powerful method for the observation of unsynchronized chemical dynamics and nanoscale behavior.[1,2] While biological structure and dynamics are rich targets for SM measurements,[3−5] nonbiological applications of SM techniques have explored diffusion,[6−9] chromatographic interactions,[10,11] adsorption and desorption behavior,[12] photoinduced electron transfer,[13,14] and photocatalysis.[15] A particularly rich abiotic application of SM microscopy has been investigation of chemical reaction kinetics at nanoparticle catalysts, including gold[16] and copper[17] nanoparticles, platinum−silica core−shell particles,[18] and inorganic nanocrystals.[19] A variety of nanoparticle reaction types have been explored, including acid and base catalysis[20,21] and redox catalysis.[22−24] Reactivity of nanoparticle catalysts, like that of enzymes,[25,26] has been observed to be highly heterogeneous.[16,18,19,27] More recently, the action of small-molecule chemical agents[28−30] and organometallic complexes[31,32] has also begun to be explored at the SM level.[33] Study of molecular catalysts by SM fluorescence microscopy promises to improve our understanding of chemical reactions by providing insight into catalyst kinetics and heterogeneity within catalyst populations. This work details a combined SM fluorescence and bulk NMR investigation into the initiation dynamics of an operational surface-supported molecular palladium catalyst. In the process we are able to correlate SM fluorescence dynamics with specific processes in the cascade of chemical steps comprising catalyst initiation, elucidating the diverse dynamics that result from the intrinsic surface heterogeneity, and describe a potential mechanism that suggests possible chemical origins of that diversity. By providing a unique, new perspective on catalyst behavior, these results help us understand the subtle differences between the action of a catalyst in solution as compared to that at a surface, and constitute important steps in the evolution of SM techniques to tackle chemical dynamics.

An ideal molecular catalyst for SM studies would have several qualities facilitating SM fluorescence microscopy. The ideal catalyst must be reliably tethered to a surface, and immobilized in the microscope sample plane. The test system must be fluorescently labeled in a way that allows the fluorescence signal to convey information on the catalyst's chemical transitions. Finally, a good catalyst for study would be stable for long periods of time in ambient conditions. For the above reasons, pyridine enhanced precatalyst, preparation, stabilization, and initiation (PEPPSI) palladium catalysts are an attractive target for SM studies. PEPPSI catalysts are employed in a variety of coupling chemistries including Suzuki−Miyaura reactions,[34−37] as well as amination[37,38] and sulfonylation[39] reactions, due to a

Received: January 11, 2016
Published: March 4, 2016

DOI: 10.1021/jacs.6b00357
J. Am. Chem. Soc. 2016, 138, 3876−3883

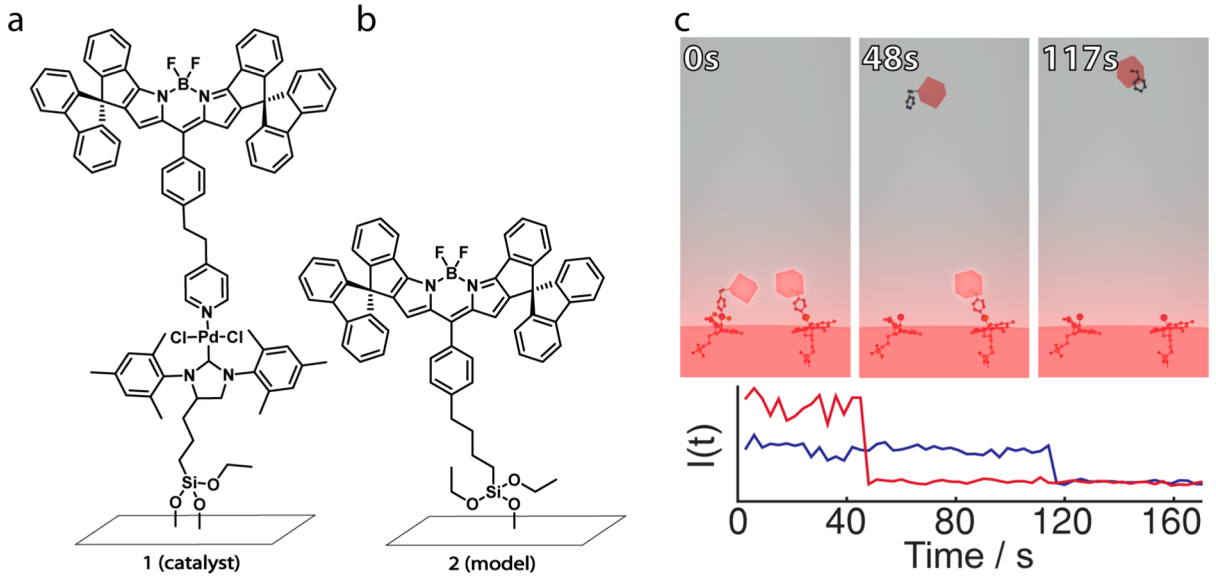

Figure 1. Single-molecule investigation of surface-supported molecular catalysts. A surface-supported, BODIPY labeled catalyst (a), or surface-supported BODIPY model compound (b), is deposited on a glass sample chamber, and viewed on a microscope. Multiple catalyst molecules are observed simultaneously (c, top left). The catalysts fluoresce (c, top) until one initiates, at which time the fluorescent ligand leaves the excitation volume and signal from that catalyst is lost (c, top middle). As multiple catalysts initiate, the fluorescence intensity traces (c, bottom, 400 μM KO*t*-Bu) from each will show a transition, providing initiation kinetics resolved at the level of individual molecules. The surface anchoring chemistry in part a is shown differently for the two molecules, representing diverse bonding configurations (see text).

combination of superior air and moisture stability[35] and high catalyst activity.[40] PEPPSI catalysts provide a convenient synthetic handle for reliable surface support through the N-heterocyclic carbene[41] and for addition of fluorescent functionality via the labile pyridine ligand.[42] Importantly, as loss of the pyridine ligand must precede formation of the active catalyst,[36] and as the ligand itself has been implicated in the remarkable stability of PEPPSI catalysts,[34] a fluorescent label at this ligand offers the opportunity to explore these important processes at the SM level.

In order to probe the initiation mechanism of the PEPPSI palladium catalyst through SM fluorescence microscopy, we have synthesized a surface-supported PEPPSI palladium catalyst functionalized with a boron-dipyrromethene (BODIPY) fluorophore appended to the pyridine ligand, **1**, Figure 1a. The fluorescent moiety provides a proxy for initiation by reporting on the presence of pyridine ligated to the palladium. BODIPY fluorophores are an attractive label for molecular catalysts due to their synthetic modularity, stability, high fluorescent quantum yield,[43] and lack of reactive nucleophilic heteroatoms, which allows the fluorophore to act as a benign spectator molecule near organometallic complexes (Supporting Information).[44] We have specifically chosen a spirofluorene functionalized BODIPY with an expanded π-system[45] as our fluorescent reporter because it enables use of red excitation, substantially reducing background photons from solvent Raman scattering and n $\rightarrow$ π^* transitions of impurities in nonaqueous solvents,[46] and the stiff spiro groups greatly improve its quantum yield relative to those of other red fluorophores.[45] As will be shown, this red BODIPY demonstrates excellent imaging properties for SM microscopy in nonaqueous protic media like 2-propanol (IPA).

In order to observe initiation of **1** under Suzuki–Miyaura coupling conditions, we conduct wide-field fluorescence microscopy employing an objective-type pseudototal internal reflectance fluorescence (TIRF) excitation mode. In TIRF, laser excitation is restricted to close proximity to the surface, making our fluorescence measurements highly surface selective.[47] In this experimental configuration (Figure 1c), BODIPY fluorophores appended to uninitiated catalyst will be fluorescent, while ligands freed during initiation will quickly diffuse out of the excitation volume and no longer emit, making fluorescence intensity a targeted probe of catalyst initiation. By controlling the surface density of catalyst molecules so that we can observe individual catalysts on the surface, we can gather kinetic information on initiation resolved at the level of single catalyst molecules (Figure 1c, bottom).

Understanding the mechanism and kinetics of initiation of surface-supported molecular catalysts is an outstanding problem in catalysis, where supported catalysts have long been discussed as potential recyclable catalysts due to their ease of recovery. Though surface–catalyst interactions can provide new avenues for reactivity,[48,49] surface-supported catalysts typically exhibit less favorable reaction kinetics or selectivity than their solution-phase analogues.[50] Quantifying initiation kinetics of surface-supported molecular catalysts is particularly challenging because the surface heterogeneity and biphasic conditions result in substantial obstacles to spectroscopy, including NMR. The rich chemical environment at a solid–liquid interface can create diverse speciation of supported catalysts that has been linked to diverse chemical activity,[51] while sluggish initiation kinetics may play a role in the reduced activity of surface-supported catalysts. Consequently, understanding the influence of the surface on catalyst behavior is critical to improvement of supported molecular catalysts.

RESULTS AND DISCUSSION

NMR Study of Initiation of a Homogeneous Catalyst.

The initiation of **1** under Suzuki–Miyaura coupling conditions is likely a multistep process[52,53] ending with a Pd^0 species capable of entering the well-known cross-coupling catalytic cycle. In order to isolate the role of each reagent on catalyst

DOI: 10.1021/jacs.6b00357
J. Am. Chem. Soc. 2016, 138, 3876–3883

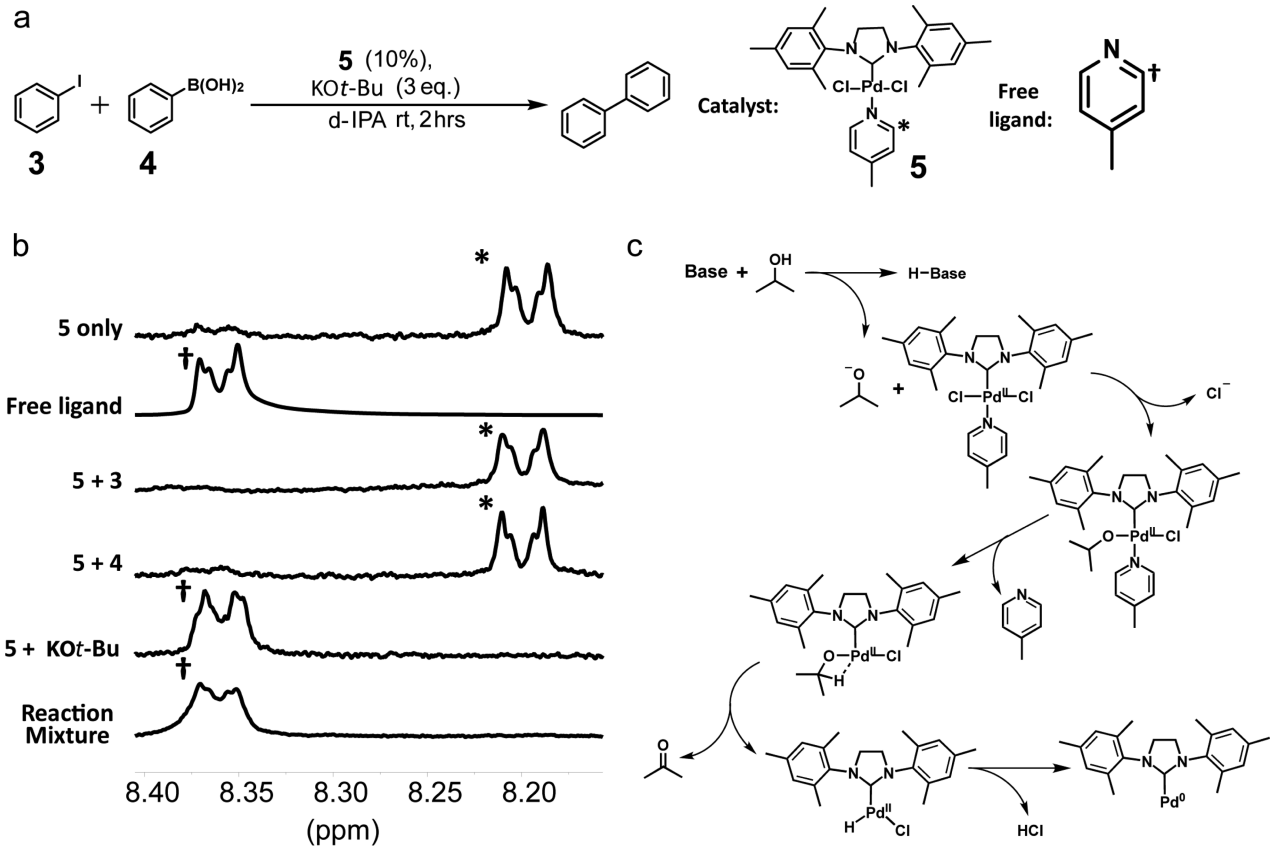

Figure 2. Initiation of **5** in deuterated IPA, reaction, and mechanism during Suzuki cross-coupling. Dissociation of the pyridine ligand from the catalyst was studied under turnover conditions (a), and upon exposure to individual reagents. Ligand dissociation results in a deshielding of the pyridinic doublets as monitored by NMR (b). NMR spectra of solutions of homogeneous catalyst (**5**) and individual reagents (**3**, **4**), as well as the full reaction mixture, show that KOtBu is both necessary and sufficient for dissociation of pyridine from **5**, consistent with an initiation mechanism driven by attack by deprotonated solvent and ending in β-hydride elimination (c). See Supporting Information for full NMR of reaction mixtures.

initiation under typical coupling conditions (Figure 2a),[34] we examined solutions containing a homogeneous, unlabeled catalyst and various combinations of reagents by NMR (Figure 2b). Addition of the reaction substrates, **3** and **4**, to the catalyst showed no shift in the NMR spectrum, indicating ligand dissociation did not occur. Addition of potassium *tert*-butoxide (KOtBu) caused the disappearance of the peaks corresponding to the pyridine bound to the catalyst, and the appearance of peaks corresponding to the free ligand. Pyridine dissociation occurred rapidly and was complete by 15 s after addition of KOtBu. Under these same conditions, deuterated acetone formation was observed after several hours, indicative of β-hydride elimination of isopropoxide (Supporting Information). Addition of all reagents also resulted in the formation of free pyridine ligand and deuterated acetone, as well as biphenyl product (Figure 2, Supporting Information). The proposed initiation mechanism is shown in Figure 2c. The IPA solvent is deprotonated by base, and the isopropoxide ion displaces a chloride ligand on the catalyst, thus lowering the activation barrier to pyridine ligand dissociation by nearly 3 kcal/mol (Supporting Information). This dissociation opens up a vacant coordination site for β-hydride elimination of isopropoxide to form acetone. Reductive elimination of HCl forms the Pd^0 active catalyst. Isopropoxide coordination followed by β-hydride elimination to form acetone has been suggested as a key step in the activation of other Pd-NHC complexes in IPA.[54]

Single-Molecule Initiation Kinetics of a Surface-Supported Catalyst. As summarized in Figure 2c and exhibited in our NMR measurements, release of the pyridine ligand into solution is a critical step along the initiation cascade, and can be used to monitor the initiation kinetics of **1** at the SM level. A sparse layer of **1** embedded in a dense layer of triethoxy(octyl)silane (TOS) was prepared on a silica surface in a specially designed all-glass reaction chamber[42] containing IPA, to form a sparse distribution of catalyst in high surface coverage of the alkyl silane. TOS slows the base-induced destruction of the silica support by creating a nonpolar barrier to base attack.[55] A large volume of IPA with KOtBu of known molarity with or without reaction substrates is quickly added, and time-lapse fluorescence images are recorded over time (example in Supporting Information). We use a home-built drift compensation system to maintain focus during and after the addition of reagent (further information in Methods and Supporting Information). The red spiro functionalized BODIPY is seen to be a stable SM emitter under these conditions (Figure 3a, Supporting Information). Individual molecules of **1** were identified, and survival times were determined using an automated algorithm (Figure 3a). The remaining fraction of surviving molecules, S, was plotted as a function of time (Figure 3b) for a series of increasing concentrations of KOtBu. Higher concentrations of base result in conspicuously nonexponential decay kinetics. Median survival times ($t_{1/2}$) are linear with the inverse of base concentration (Figure 3c, inset), indicative of a first order decay process.

DOI: 10.1021/jacs.6b00357
J. Am. Chem. Soc. 2016, 138, 3876−3883

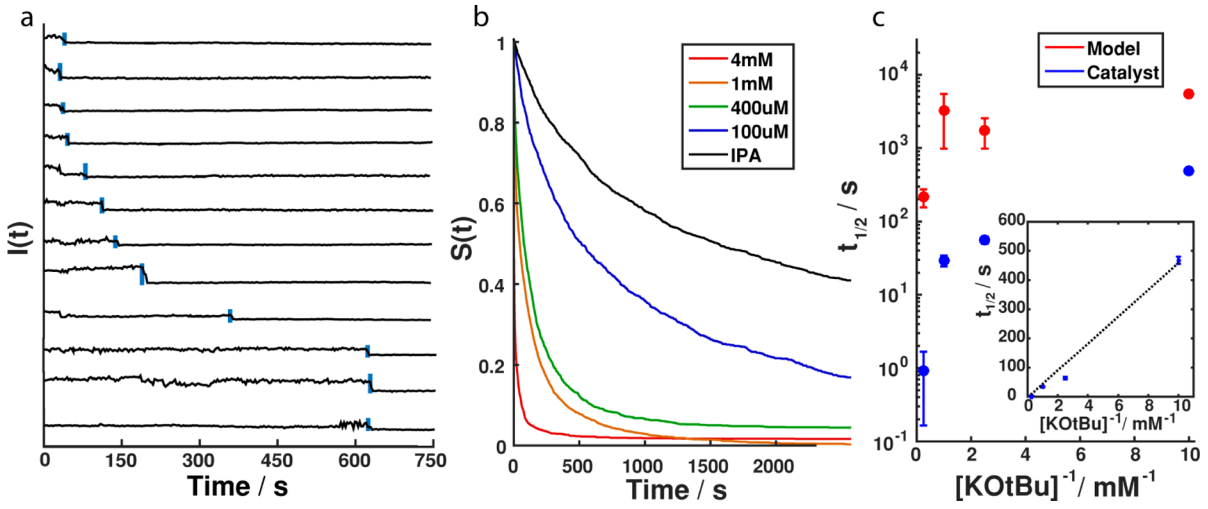

Figure 3. Extraction of SM kinetics. In an automated process, time/fluorescence trajectories from individual catalysts (a, black) are isolated from video of a sparse catalyst-coated surface, and the frame where the fluorescence is lost (blue line) is found for each. (b) The surviving fraction $S(t)$, aggregated from initiation of many (>1000) molecules, shows conspicuously stretched exponential behavior at high [KOtBu], visible as an elbow in the decay. Median lifetimes (which reflect the broad distribution of component rates, see Supporting Information) of **1** and **2** were well-separated across the concentration range studied (c). Median lifetimes are roughly linear vs $[\mathrm{KOtBu}]^{-1}$ (c, inset), indicative of first order behavior. Because the concentration of catalyst is small compared to concentration of base, [KOtBu] is expected to remain constant over the course of the experiment. Traces in part a are taken from a single video of 400 μM base addition. The 10 M^{-1} lifetime of the model compound has a large uncertainty due to our observation window being less than half of the median lifetime. The error bar for this point was omitted for clarity of the logarithmic plot.

While loss of the fluorescently labeled ligand due to catalyst initiation will result in loss of the SM fluorescence signal, other loss mechanisms must also be considered. In order to ascertain the contributions of photobleaching, as well as lysis of the surface anchoring functionality, which could also result in loss of fluorescence, we measured **2**, in which the BODIPY is covalently bound to the surface support with the same anchoring functionality as **1**, under similar conditions to **1**. The median survival times of **2** were found to be 1−2.5 orders of magnitude greater than those of **1** (Figure 3c), indicating a significant separation of time scales of catalyst initiation (fast) and combined destruction of the surface support and photobleaching (slow). The mixing time of solution in the sample chamber, blinking of the BODIPY fluorophore, and presence of fluorescent impurities were all considered as possible confounding processes in our experiment, and determined to be minor contributors (Supporting Information). Consequently, catalyst initiation can be viewed as the dominant mechanism of fluorescence loss, and fluorescence loss can be used as a proxy for catalyst initiation.

The highly non-monoexponential kinetics of catalyst initiation were investigated by Weibull analysis,[56,57] a technique widely used in reliability engineering, to model S with the stretched exponential form shown in eq 1.

$$S(t) = \mathrm{e}^{-(k_{\mathrm{eff}}t)^{\beta}} \tag{1}$$

$$\ln(-\ln(S(t))) = \beta \ln t - \beta \ln\left(\frac{1}{k_{\mathrm{eff}}}\right) \tag{2}$$

In Weibull analysis, S is linearized on a Weibull plot as eq 2, and the shape parameter β and scale parameter (effective rate constant) k_{eff} of the Weibull distribution are extracted from the slope and intercept of the linear fit, respectively. Monoexponential kinetics are revealed as lines with a slope of 1 (Figure 4a, dashed gray line), while stretched exponential behavior is indicated by $\beta < 1$, with lower β values easily seen as lines approaching horizontal and indicative of increasingly broad distributions of rates. The distribution of survival times of **1** after addition of KOtBu in IPA (Figure 4a) is well-approximated by the linearized fit shape. β decreases with increasing base concentration both when only base is added (Figure 4b) and under turnover conditions (Figure 4c). Decay dynamics of **2** also show a decreasing shape parameter (Supporting Information), albeit at substantially reduced rate constants. Though catalysts show the same qualitative trend (Figure 4b,c) with and without the inclusion of the arylhalide **3** and arylboronic acid **4**, we will focus our analysis on the base addition without additional reagents due to a lower concentration of fluorescent impurities. Additional discussion of behavior in the presence of **3** and **4** is presented as Supporting Information.

Stretched exponential kinetics can be viewed as deriving from a continuous distribution, $H(k)$, of monoexponential processes.[58,59]

$$\mathrm{e}^{-(k_{\mathrm{eff}}t)^{\beta}} = \int_0^{\infty} H(k)\mathrm{e}^{-tk}\,\mathrm{d}k \tag{3}$$

Smaller values of β indicate a greater dispersion of rate constants. The inverse relationship between base concentration and β indicates increasing spread in the relative rate constant distribution and greater heterogeneity of catalyst behavior with addition of base. This changing distribution, $H(k)$, can be directly visualized (Figure 4d), with $H(k)$ approaching a singular value as β approaches unity.

Physical Interpretation of Stretched Decays. Surface-supported molecular catalysts inhabit environments that are significantly more complex than their homogeneous analogues due to the variety of surface microenvironments. On silica support, this variety begins with the distribution of silanol sites across the silica surface,[51] leading to a wide range of possible attachment configurations for the surface-supported catalyst. In addition, while the catalyst is extremely dilute during the deposition, the high concentration of TOS in the deposition

DOI: 10.1021/jacs.6b00357
J. Am. Chem. Soc. 2016, 138, 3876−3883

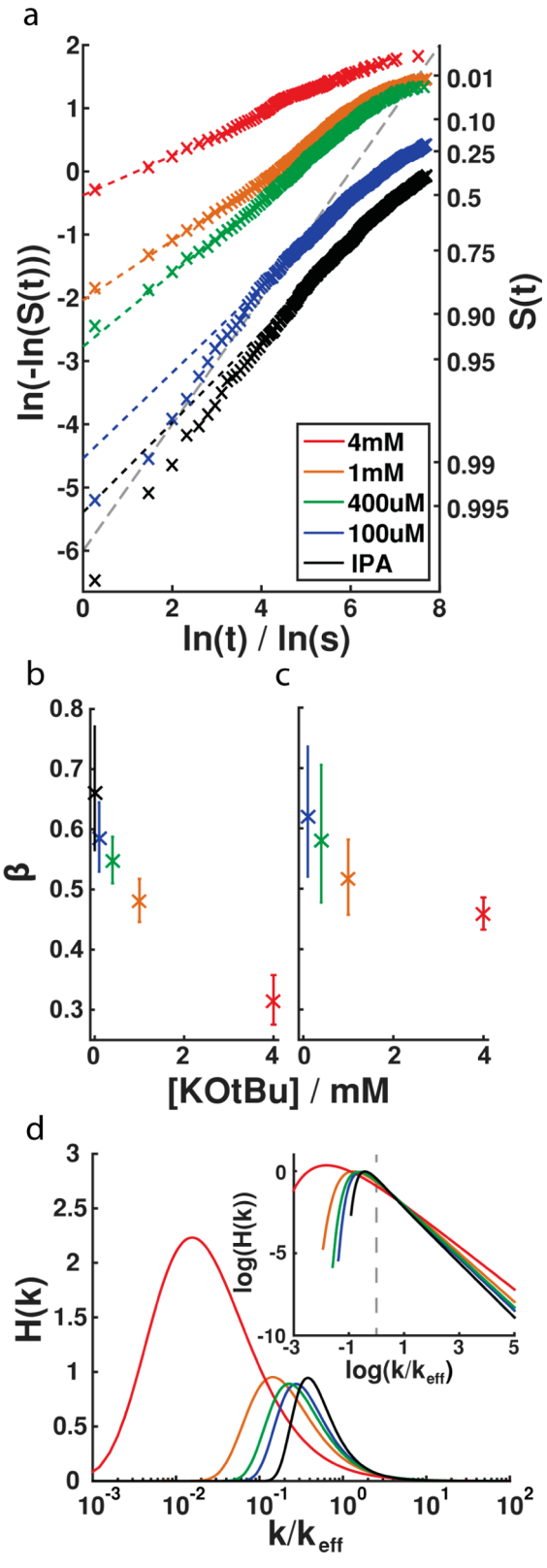

Figure 4. Analysis of stretched exponential behavior with the Weibull distribution. Survival fractions after base addition to catalyst in IPA (a, X) are well-fit by lines with slope less than 1 (- - -) on a Weibull plot (a), indicative of stretched exponential behavior. A line on the Weibull plot with slope 1 (gray - - -) would indicate a monoexponential decay. Deviation from linearity at early times in the low concentration data accounts for <10% of catalyst molecules (right axis). Examination of the shape parameter (slope), β, for the catalyst with base (b) and catalyst under turnover conditions (c) shows similar trends of decreasing β, suggesting similar drivers of heterogeneity. The trend in β indicates a broadening distribution of rates (d, calculated from β in b). At low β (red), both extremely fast and extremely slow rates are more common than in distributions with high β (black). At $\beta = 1$ (gray - - -), the distribution of exponential rates becomes a delta function (monoexponential) at k_{eff} (inset d).

solution could allow silane groups to coalesce and condense homogeneously,[60] leading to deposition at the surface of a variety of large catalyst−silane clusters, largely nonpolar layers that may pose a significant obstacle to the polar isopropoxide. The range of attachment cluster sizes and geometries, as well as the range of attachment chemistries of those clusters, leads to a highly polymorphous catalyst microenvironment. Moreover, a variety of conformations adopted by the catalysts' flexible alkyl tether can lead to a variety of orientations relative to the surface. Because these microenvironments influence the isopropoxide base's approach to and interaction with the catalyst metal center, the surface heterogeneity will be reflected in the catalyst behavior, including initiation. Critically, though the existence of structural heterogeneity at the surface has been verified by other experimental approaches,[51] our investigation constitutes the first direct observation of the effect of the molecular catalyst *structural* heterogeneity on the catalyst *dynamics*. That effect is encapsulated in the increasing spread of rates in Figure 4d.

That a diversity of microenvironments would yield a corresponding diversity of initiation dynamics is anticipated. The unexpected element of Figure 4 is that the apparent diversity *increases* as a function of base concentration. If the heterogeneous dynamics stem from the heterogeneity in microenvironments, then a single underlying structural distribution, largely independent of base concentration, must be capable of yielding increasingly heterogeneous dynamics under different chemical conditions. Said another way, the structural diversity may be nearly constant in all samples, but the dynamics *appear* to be increasingly heterogeneous at high base concentrations, despite likely deriving from the same underlying family of structures.

Saturation kinetics of the catalyst can give rise to the increasingly wide distribution of rates we observe. In a saturation model, the presence of a diversity of maximum rates will yield highly monodisperse rates below the saturation point, but a broadening distribution of rates as individual catalysts near saturation. In this mechanism, a single underlying distribution of saturation points can yield a variety of narrow or broad distributions of behaviors. The geometry of the surface is extremely conducive to the creation of saturation kinetics. Molecular dynamics simulations of alkane functionalized silica surfaces have shown a highly disordered network of surface-supported alkanes, with pockets of low alkane density as well as dense patches.[61] Pockets in the immediate vicinity of catalyst molecules constitute positions proximal to the catalyst available for occupation by polar isopropoxide molecules, with pockets of different size leading to differences in the number of total available positions, while the position and shape of the pockets can modulate base activity. Because isopropoxide molecules (B) must first occupy these entry sites (A) before reacting with the catalyst, reforming an empty entrance site next to an initiated catalyst (A′) and releasing pyridine (i.e., a two-step

DOI: 10.1021/jacs.6b00357
J. Am. Chem. Soc. 2016, 138, 3876−3883

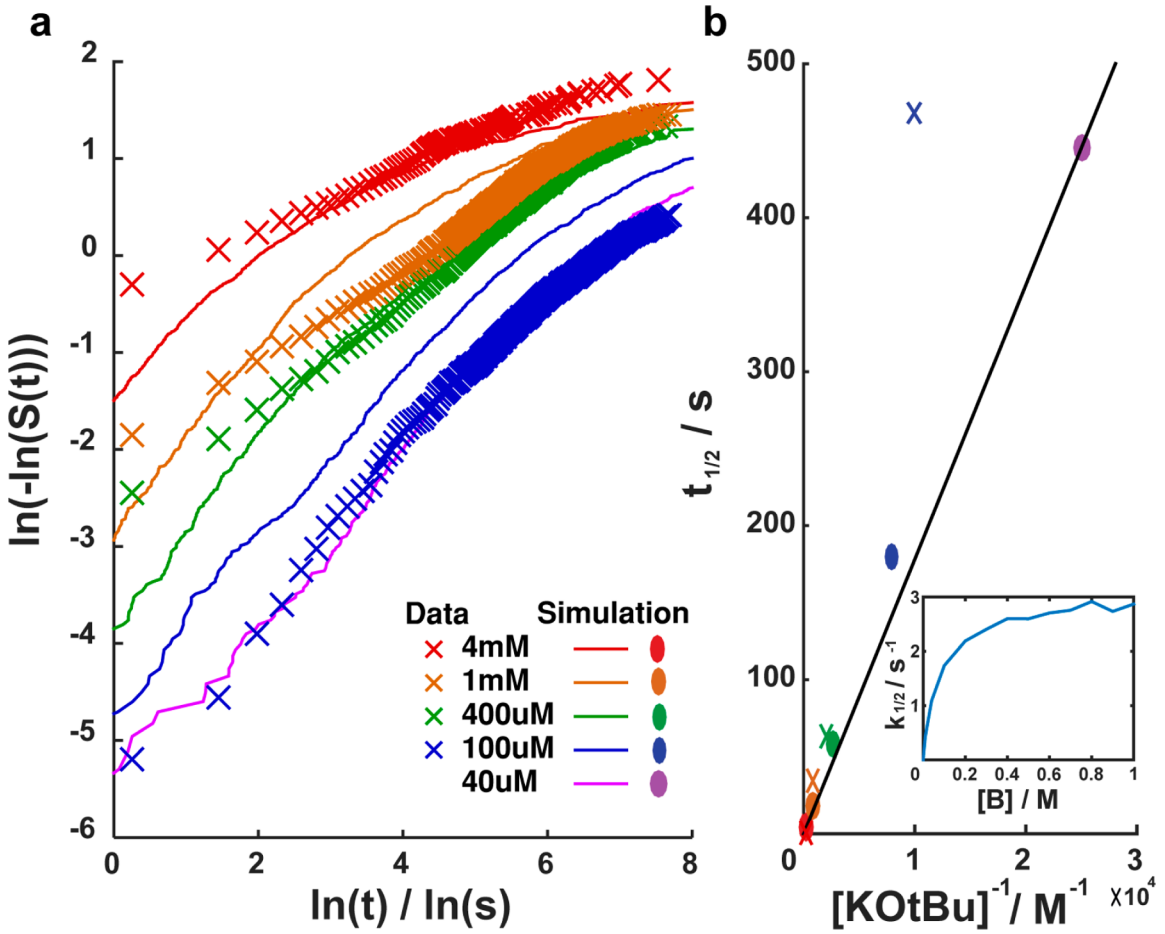

Figure 5. Simulation of survival times with distributions in k_2 and $[A]_T$. Simulated data (a, solid) qualitatively match experimental data (×), capturing the inverse relationship between slope (β) and concentration. Due to the double-log y-axis, points below −2 account for <10% of the population. In the simulation, a marginally greater range of concentrations is needed to observe the change in lifetime in our data (purple line). First order dependence on [KOtBu] is preserved over the critical range in the simulation (b), albeit with a different slope. Deviations are most conspicuous at low [KOtBu]. Closer agreement between the observed and simulated data for both parts a and b could be obtained by also including distributions of values for k_1 and k_{-1}. Extension of the simulated bulk kinetics to substantially higher base concentrations shows the expected saturation behavior (b, inset). Simulations were generated on the basis of eq 5 with $k_1 = 20\ s^{-1}\ M^{-1}$ and $k_{-1} = 1 \times 10^{-8}\ s^{-1}$. A Weibull distribution ($\tau = 3.5$, $\beta = 0.9$) was randomly sampled to generate $[A]_T$, as well as k_2 ($\tau = 2$, $\beta = 0.9$). Other types of distributions, as well as distributions in other variables, led to poorer fits (Supporting Information).

mechanism), and because there are a limited number of sites available due to the dense foliage of alkane surrounding the catalyst, saturation behavior will be observed (functionally equivalent to a Langmuir–Hinshelwood mechanism[16] or Michaelis–Menten kinetics,[26] which have both been explored at the SM level)

$$A + B \underset{k_1}{\overset{k_1}{\rightleftharpoons}} AB \xrightarrow{k_2} A' + C \tag{4}$$

$$R_{obs} = \frac{k_2[A]_T[B]}{\frac{k_{-1}+k_2}{k_1} + [B]} \tag{5}$$

where k_1 and k_{-1} are the rates at which isopropoxide (B) diffuses into and out of sites (A) in the alkane pocket surrounding the catalyst with total number of sites $[A]_T$, k_2 is the rate constant of initiation of the precatalyst complex once the isopropoxide enters the pocket, and R_{obs} is the observed reaction rate. As will be shown, eq 5 provides a means of generating our observed kinetic distributions, with heterogeneity arising naturally as some species are limited by the first step (k_1) while others are limited by the second step (k_2). Under these conditions, the order of R_{obs} with respect to base will be first order at low base concentrations, and become zeroth order at high concentration as the average occupancy of the pocket increases. However, with singular values for all of the component rate constants, a Weibull plot will show a series of parallel lines with slope, $\beta = 1$ (monoexponential decay), with curves coalescing as saturation is approached (Supporting Information), contrary to our observations.

In order for the slope of the Weibull plot to decrease with increasing base concentration, as observed, there must be a distribution of maximum rates among catalysts. In such a system, the distribution of observed rates will broaden as an increasing fraction of the catalysts approach saturation, leading to a change in the slope of the associated Weibull plot. Critically, a distribution of values of only certain parameters in eq 5 are capable of providing the observed rate dependence, thus reporting on the microscopic origins of the macroscopic diversity. Conceptually, we can imagine the changing distributions derived from eq 5 as a transitioning of catalysts

DOI: 10.1021/jacs.6b00357
J. Am. Chem. Soc. 2016, 138, 3876–3883

operating in the high versus low concentration regime. At high concentrations of base, the model approaches eq 6

$$R_{obs} = k_2[A]_T \quad (6)$$

while at low concentration, the saturation model approaches eq 7, for small k_{-1}.

$$R_{obs} = k_1[A]_T[B] \quad (7)$$

A distribution of values of k_1 would lead to behavior opposite to that observed, with a broad distribution of rates at low base concentrations (eq 7) that narrows at high concentrations (eq 6). In contrast, a distribution of k_2 will lead to a broadening distribution of rates for large [B]. However, because the distribution does not exhibit monoexponential behavior at any concentration over the range studied (Figure 5), a distribution of either $[A]_T$ or k_1 is also required. Simulations generated from distributions in k_1 and k_2 did not generate the magnitude of change in β seen in our data over a similar concentration range, suggesting distributions of $[A]_T$ and k_2 are responsible for the observed catalyst kinetics (Figure 5). Critically, while distributions in the parameters generate the observed distributions in our kinetics, in this same regime, the rate will still be first order in [B], preserving the observed bulk behavior with regard to base (Figure 5b). At substantially higher concentrations, the process shifts to zero order in base, consistent with eq 6 (Figure 5b, inset).

We interpret k_2 as relating to variations in catalyst rate constant due to changes in the local microenvironment, and $[A]_T$ as a measure of the maximum attainable local concentration of isopropoxide at the palladium center of **1**. This maximum local concentration is controlled by the crowding of the local catalyst environment by TOS. Because the contour length of TOS is longer than the contour length of the tether on **1**, the alkyl chains can be expected to rise above the metal center of the catalyst. The environment around each catalyst will be heterogeneous and greasy, with local density of alkyl chains creating a unique solvent compartment around each catalyst. This range of local geometries can create differences in permeability of the alkane layer (k_1), differences in the maximum achievable local concentration of base ($[A]_T$), and also differences in accessibility of the metal center to base due to steric effects and differences in activated complex stability as the steric crowding of the bulky activated precatalyst changes from site to site (both reflected in k_2). This model of hindered attack can also explain the changing shape parameter in model **2** (Supporting Information), where base-assisted destruction of the silyl ether attachment group will depend on accessibility of the support surface to isopropoxide in the same way the catalyst kinetics depend on accessibility of the metal. Because the majority of observed heterogeneity can be generated with a distribution in $[A]_T$ alone (Supporting Information), we view barriers to isopropoxide attack due to a limited number of available entry sites for isopropoxide, as the main driver of catalyst heterogeneity.

CONCLUSIONS

We have described the first combined SM and bulk investigation of organometallic catalyst initiation. The initiation kinetics were observed to be highly heterogeneous and grew more heterogeneous with increasing base concentration, and this increasing heterogeneity was shown to be consistent with a saturation model that includes the need to access a limited number of entry sites. More broadly, population diversity in catalysts has important implications to a wide range of reactions, where inactive subpopulations could significantly slow bulk reaction kinetics. For example, our results indicate that this highly heterogeneous distribution of observed rates at high base concentrations includes a significant population of slow-initiating species, even as the majority initiates quickly. To better characterize the way in which the attachment chemistry affects the catalyst heterogeneity, catalysts linked by more rigid or longer tethers could be compared to this study. Further study of catalyst initiation could provide insight into causes of catalyst inefficiency and failure by allowing us to create a more detailed model of supported catalyst behavior that includes this diversity. Our approach is applicable to a wide variety of surface-supported catalysts, including electrocatalysts, and will be particularly powerful when paired with a means of monitoring individual turnover events,[16,25] where the presence or absence of specific ligands can be correlated with reactivity. Use of a FRET labeled catalyst would enable independent observation of both ligand and catalyst, potentially allowing observation of ligand return dynamics. Insight into truly homogeneous catalyst behavior will require careful control of surface−catalyst interactions to reduce the surface influence, a process we are currently exploring. In total, SM techniques hold the potential to be a powerful new addition to the toolkit for mechanistic investigation of organometallic species.

METHODS

Synthesis. Full synthetic details are given in the Supporting Information. 4-Ethynylpyridine[62] was obtained in 90% yield, and the brominated red BODIPY fluorophore[45] was obtained in 38% yield by following literature procedures. Sonogashira coupling between the alkyne and aryl halide (35% yield), followed by hydrogenation (58% yield), yielded the PEPPSI ligand. Following an earlier procedure,[42] compound **1** was prepared from the PEPPSI ligand and a functionalized Pd dimer by refluxing in DCM at elevated temperature (44% yield).

Fluorescence Microscopy. Full details on the experimental setup are given in the Supporting Information. We performed SM fluorescence microscopy on an inverted microscope with 633 nm excitation provided in a pseudo-TIRF geometry. An electronic shutter chopped excitation light for time-lapse imaging. The camera recorded a 100 ms exposure every 3 s. An active drift compensation routine was used to dampen focal shifts upon reagent addition and maintain focus for prolonged periods by mapping focal drift onto the spatial displacement of the reflected TIRF beam as it leaves the back aperture of the microscope as observed on a camera.

ASSOCIATED CONTENT

Supporting Information

The Supporting Information is available free of charge on the ACS Publications website at DOI: 10.1021/jacs.6b00357.

Additional experimental details; absorption and emission spectra of BODIPY labeled molecules **1** and **2**; discussion of possible confounders including solution mixing, camera frame rate, single-molecule blinking, solvent impurities; catalyst behavior in the presence of coupling reagents; robustness of fit parameters; method of data calculation; NMR of numbered compounds (PDF)

Example time-lapse video (AVI)

AUTHOR INFORMATION

Corresponding Author

*rhg@chem.wisc.edu

DOI: 10.1021/jacs.6b00357
J. Am. Chem. Soc. 2016, 138, 3876−3883

Notes

The authors declare no competing financial interest.

■ ACKNOWLEDGMENTS

This work was supported by the National Science Foundation under Grant No. (CHE-1254936). We gratefully acknowledge partial support of this research by NSF through the University of Wisconsin Materials Research Science and Engineering Center (DMR-1121288), and would like to thank Margaret Robinson for invaluable help with surface attachment strategy.

■ REFERENCES

(1) Janssen, K. P.; De Cremer, G.; Neely, R. K.; Kubarev, A. V.; Van Loon, J.; Martens, J. A.; De Vos, D. E.; Roeffaers, M. B.; Hofkens, J. *Chem. Soc. Rev.* **2014**, *43*, 990.
(2) Moerner, W. E. *Angew. Chem., Int. Ed.* **2015**, *54*, 8067.
(3) Joo, C.; Balci, H.; Ishitsuka, Y.; Buranachai, C.; Ha, T. *Annu. Rev. Biochem.* **2008**, *77*, 51.
(4) Xie, X. S.; Choi, P. J.; Li, G. W.; Lee, N. K.; Lia, G. *Annu. Rev. Biophys.* **2008**, *37*, 417.
(5) Deniz, A. A.; Mukhopadhyay, S.; Lemke, E. A. *J. R. Soc., Interface* **2008**, *5*, 15.
(6) Zurner, A.; Kirstein, J.; Doblinger, M.; Brauchle, C.; Bein, T. *Nature* **2007**, *450*, 705.
(7) Liao, Y.; Yang, S. K.; Koh, K.; Matzger, A. J.; Biteen, J. S. *Nano Lett.* **2012**, *12*, 3080.
(8) Werley, C. A.; Moerner, W. E. *J. Phys. Chem. B* **2006**, *110*, 18939.
(9) Higgins, D. A.; Park, S. C.; Tran-Ba, K. H.; Ito, T. *Annu. Rev. Anal. Chem.* **2015**, *8*, 193.
(10) Kisley, L.; Chen, J.; Mansur, A. P.; Shuang, B.; Kourentzi, K.; Poongavanam, M. V.; Chen, W. H.; Dhamane, S.; Willson, R. C.; Landes, C. F. *Proc. Natl. Acad. Sci. U. S. A.* **2014**, *111*, 2075.
(11) Cooper, J. T.; Peterson, E. M.; Harris, J. M. *Anal. Chem.* **2013**, *85*, 9363.
(12) Kastantin, M.; Walder, R.; Schwartz, D. K. *Langmuir* **2012**, *28*, 12443.
(13) Rao, V. G.; Dhital, B.; Lu, H. P. *Chem. Commun.* **2015**, *51*, 16821.
(14) Jin, S.; Lian, T. *Nano Lett.* **2009**, *9*, 2448.
(15) Tachikawa, T.; Yamashita, S.; Majima, T. *J. Am. Chem. Soc.* **2011**, *133*, 7197.
(16) Xu, W.; Kong, J. S.; Yeh, Y. T.; Chen, P. *Nat. Mater.* **2008**, *7*, 992.
(17) Decan, M. R.; Impellizzeri, S.; Marin, M. L.; Scaiano, J. C. *Nat. Commun.* **2014**, *5*, 4612.
(18) Han, R.; Ha, J. W.; Xiao, C.; Pei, Y.; Qi, Z.; Dong, B.; Bormann, N. L.; Huang, W.; Fang, N. *Angew. Chem., Int. Ed.* **2014**, *53*, 12865.
(19) Roeffaers, M. B.; Sels, B. F.; Uji-i, H.; De Schryver, F. C.; Jacobs, P. A.; De Vos, D. E.; Hofkens, J. *Nature* **2006**, *439*, 572.
(20) Roeffaers, M. B. J.; De Cremer, G.; Libeert, J.; Ameloot, R.; Dedecker, P.; Bons, A.-J.; Bückins, M.; Martens, J. A.; Sels, B. F.; De Vos, D. E.; Hofkens, J. *Angew. Chem., Int. Ed.* **2009**, *48*, 9285.
(21) Liu, K.-L.; Kubarev, A. V.; Van Loon, J.; Uji-i, H.; De Vos, D. E.; Hofkens, J.; Roeffaers, M. B. J. *ACS Nano* **2014**, *8*, 12650.
(22) Ristanović, Z.; Kerssens, M. M.; Kubarev, A. V.; Hendriks, F. C.; Dedecker, P.; Hofkens, J.; Roeffaers, M. B. J.; Weckhuysen, B. M. *Angew. Chem., Int. Ed.* **2015**, *54*, 1836.
(23) Martínez, V. M.; Cremer, G. D.; Roeffaers, M. B. J.; Sliwa, M.; Baruah, M.; De Vos, D. E.; Hofkens, J.; Sels, B. F. *J. Am. Chem. Soc.* **2008**, *130*, 13192.
(24) Sambur, J. B.; Chen, T. Y.; Choudhary, E.; Chen, G. Q.; Nissen, E. J.; Thomas, E. M.; Zou, N. M.; Chen, P. *Nature* **2016**, *530*, 77.
(25) English, B. P.; Min, W.; van Oijen, A. M.; Lee, K. T.; Luo, G.; Sun, H.; Cherayil, B. J.; Kou, S. C.; Xie, X. S. *Nat. Chem. Biol.* **2006**, *2*, 87.
(26) Lu, H. P.; Xun, L.; Xie, X. S. *Science* **1998**, *282*, 1877.
(27) Xu, W.; Kong, J. S.; Chen, P. *J. Phys. Chem. C* **2009**, *113*, 2393.
(28) Rybina, A.; Thaler, B.; Kramer, R.; Herten, D. P. *Phys. Chem. Chem. Phys.* **2014**, *16*, 19550.
(29) Rybina, A.; Lang, C.; Wirtz, M.; Grussmayer, K.; Kurz, A.; Maier, F.; Schmitt, A.; Trapp, O.; Jung, G.; Herten, D. P. *Angew. Chem., Int. Ed.* **2013**, *52*, 6322.
(30) Ameloot, R.; Roeffaers, M.; Baruah, M.; De Cremer, G.; Sels, B.; De Vos, D.; Hofkens, J. *Photochem. Photobiol. Sci.* **2009**, *8*, 453.
(31) Esfandiari, N. M.; Wang, Y.; Bass, J. Y.; Blum, S. A. *Inorg. Chem.* **2011**, *50*, 9201.
(32) Esfandiari, N. M.; Blum, S. A. *J. Am. Chem. Soc.* **2011**, *133*, 18145.
(33) Cordes, T.; Blum, S. A. *Nat. Chem.* **2013**, *5*, 993.
(34) Nasielski, J.; Hadei, N.; Achonduh, G.; Kantchev, E. A.; O'Brien, C. J.; Lough, A.; Organ, M. G. *Chem. - Eur. J.* **2010**, *16*, 10844.
(35) Dash, C.; Shaikh, M. M.; Ghosh, P. *Eur. J. Inorg. Chem.* **2009**, *2009*, 1608.
(36) O'Brien, C. J.; Kantchev, E. A.; Valente, C.; Hadei, N.; Chass, G. A.; Lough, A.; Hopkinson, A. C.; Organ, M. G. *Chem. - Eur. J.* **2006**, *12*, 4743.
(37) Kirschning, A.; Mennecke, K. *Synthesis* **2008**, *2008*, 3267.
(38) Organ, M. G.; Abdel-Hadi, M.; Avola, S.; Dubovyk, I.; Hadei, N.; Kantchev, E. A.; O'Brien, C. J.; Sayah, M.; Valente, C. *Chem. - Eur. J.* **2008**, *14*, 2443.
(39) Sayah, M.; Organ, M. G. *Chem. - Eur. J.* **2011**, *17*, 11719.
(40) Larrosa, I.; Somoza, C.; Banquy, A.; Goldup, S. M. *Org. Lett.* **2011**, *13*, 146.
(41) Phan, N. T. S.; Van Der Sluys, M.; Jones, C. W. *Adv. Synth. Catal.* **2006**, *348*, 609.
(42) Upadhyay, S. P.; Lupo, K. M.; Marquard, A. N.; Ng, J. D.; Bates, D. M.; Goldsmith, R. H. *J. Phys. Chem. C* **2015**, *119*, 19703.
(43) Loudet, A.; Burgess, K. *Chem. Rev.* **2007**, *107*, 4891−4932.
(44) Canham, S.; Bass, J.; Navarro, O.; Lim, S.-G.; Das, N.; Blum, S. A. *Organometallics* **2008**, *27*, 2172.
(45) Kowada, T.; Yamaguchi, S.; Ohe, K. *Org. Lett.* **2010**, *12*, 296.
(46) Moerner, W. E.; Fromm, D. P. *Rev. Sci. Instrum.* **2003**, *74*, 3597.
(47) Martin-Fernandez, M. L.; Tynan, C. J.; Webb, S. E. *J. Microsc.* **2013**, *252*, 16.
(48) Notestein, J. M.; Katz, A. *Chem. - Eur. J.* **2006**, *12*, 3954.
(49) Canlas, C. P.; Lu, J.; Ray, N. A.; Grosso-Giordano, N. A.; Lee, S.; Elam, J. W.; Winans, R. E.; Van Duyne, R. P.; Stair, P. C.; Notestein, J. M. *Nat. Chem.* **2012**, *4*, 1030.
(50) Madhavan, N.; Jones, C. W.; Weck, M. *Acc. Chem. Res.* **2008**, *41*, 1153.
(51) Coperet, C.; Chabanas, M.; Saint-Arroman, R. P.; Basset, J.-M. *Angew. Chem., Int. Ed.* **2003**, *42*, 156.
(52) Steinhoff, B. A.; Guzei, I. A.; Stahl, S. S. *J. Am. Chem. Soc.* **2004**, *126*, 11268.
(53) Schultz, M. J.; Adler, R. S.; Zierkiewicz, W.; Primalov, T.; Sigman, M. S. *J. Am. Chem. Soc.* **2005**, *127*, 8499.
(54) Singh, R.; Viciu, M. S.; Kramareva, N.; Navarro, O.; Nolan, S. P. *Org. Lett.* **2005**, *7*, 1829.
(55) Schunk, T. C. *J. Chromatogr. A* **1993**, *656*, 289.
(56) Abernethy, R. B.; Breneman, J. E.; Medlin, C. H.; Reinman, G. L. *Weibull Analysis Handbook*; United Technologies Corporation, 1983.
(57) Flomenbom, O.; Velonia, K.; Loos, D.; Masuo, S.; Cotlet, M.; Engelborghs, Y.; Hofkens, J.; Rowan, A. E.; Nolte, R. J.; Van der Auweraer, M.; de Schryver, F. C.; Klafter, J. *Proc. Natl. Acad. Sci. U. S. A.* **2005**, *102*, 2368.
(58) Lindsey, C. P.; Patterson, G. D. *J. Chem. Phys.* **1980**, *73*, 3348.
(59) Berberan-Santos, M. N.; Bodunov, E. N.; Valeur, B. *Chem. Phys.* **2005**, *315*, 171.
(60) Witucki, G. L. *J. Coating. Technol. Res.* **1993**, *65*, 57.
(61) Lippa, K. A.; Sander, L. C. *J. Chromatogr. A* **2006**, *1128*, 79.
(62) Moreno-Garcia, P.; Gulcur, M.; Manrique, D. Z.; Pope, T.; Hong, W.; Kaliginedi, V.; Huang, C.; Batsanov, A. S.; Bryce, M. R.; Lambert, C.; Wandlowski, T. *J. Am. Chem. Soc.* **2013**, *135*, 12228.

DOI: 10.1021/jacs.6b00357
J. Am. Chem. Soc. 2016, 138, 3876−3883